Stieltjes imaging method for computation of oscillator-strength distributions for complex atoms*

R. K. Nesbet
IBM Research Laboratory, San Jose, California 95193
(Received 24 March 1976)

The Stieltjes imaging method makes possible the computation of photoionization or photodetachment cross sections without use of electronic continuum wave functions. Several practical difficulties are encountered in applying this method to complex atoms. Modifications of the computational procedure are introduced here, allowing the efficient computation of high-order principal representations of oscillator-strength distributions of complex atoms without numerical instabilities inherent in previous methods. Illustrative calculations are reported for the ground states of He and B. Principal representations obtained by variational calculations for these two atoms are used to compute spectroscopic moments and Van der Waals constants, and to reconstruct the oscillator strengths of line spectra at observed excitation wavelengths. Good agreement is found with all available quantitative data. **Difficulties** in constructing the photoionization cross section from the computed principal representations are shown, analyzed, and tentatively resolved by separating the oscillator-strength distributions into physically distinct excitation series.

I. INTRODUCTION

The interaction of unpolarized electric dipole radiation with an atom or molecule can be described in terms of the complex-valued polarizability function

$$\alpha(z) = \int_0^\infty \frac{df(\epsilon)}{\epsilon^2 - z^2}, \tag{1}$$

defined as a Stieltjes integral over the oscillator-strength distribution $df(\epsilon)$. Here ϵ is an excitation energy (in Hartree units, e^2/a_0, to give α in units of a_0^3) and z is a complex excitation energy or frequency variable. The complex function $\alpha(z)$ has a branch point at the ionization threshold $\epsilon_{\rm th}$. Along the branch cut for real z from $\epsilon_{\rm th}$ to $+\infty$ the imaginary part of $\alpha(z)$ is proportional to the total photoionization cross section. For all real z the real part of $\alpha(z)$ is the physical electric dipole polarizability function, with poles at discrete excitation energies.

Langhoff[1] has proposed an elegant procedure for constructing the photoionization cross section from an approximate spectral representation of $\alpha(z)$. This makes it possible to compute photoionization cross sections without the use of continuum wave functions. This procedure has been applied successfully to photoionization[2,3] of He, and to H^- photodetachment.[4,5]

The method makes use of a *principal representation* of the oscillator-strength distribution, such that $\alpha(z)$ is approximated by a finite sum

$$\alpha(z) \simeq \sum_{a=1}^{n} \frac{f_a}{\epsilon_a^2 - z^2}. \tag{2}$$

If $2n$ values of the moments

$$\mu_k = \int_0^\infty \epsilon^{-k}\, df(\epsilon) \tag{3}$$

are known, the n pairs of parameters (ϵ_a, f_a) of the corresponding principal representation are determined so that

$$\mu_k = \sum_{a=1}^{n} f_a \epsilon_a^{-k}, \quad k = 0, \ldots, 2n-1. \tag{4}$$

From a given principal representation, the cumulative oscillator-strength function

$$F(\epsilon) = \int_0^\epsilon df(\epsilon) \tag{5}$$

is approximated by the histogram

$$F(\epsilon) = \sum_{\epsilon_a < \epsilon} f_a, \quad \epsilon \neq \epsilon_a. \tag{6}$$

The values associated with rise points ϵ_a,

$$F(\epsilon_a) = \tfrac{1}{2}[F(\epsilon_a -) + F(\epsilon_a +)], \tag{7}$$

converge to $F(\epsilon)$ in the limit of large n.[6] In the ionization continuum, a continuous and non-negative oscillator-strength distribution function is defined by

$$g(\epsilon) = \frac{dF}{d\epsilon}, \tag{8}$$

such that

$$df(\epsilon) = g(\epsilon)d\epsilon. \tag{9}$$

The total photoionization cross section is[7]

$$\sigma_{\rm PI}(\epsilon) = 2\pi^2 \alpha g(\epsilon), \tag{10}$$

in units of a_0^2 if ϵ is in Hartree units, and α is the fine-structure constant.

The Stieltjes imaging method proposed by Langhoff[1] approximates $g(\epsilon)$ in the form of a histogram obtained by differentiating the piecewise linear function defined by connecting values of $F(\epsilon_a)$ given by Eq. (7) with straight-line segments.[8]

Smooth curves obtained from such histograms are compared with experimental photoionization cross sections.[2-4]

The present paper reports preliminary results of an investigation of the applicability of this method to complex atoms. Several practical difficulties were encountered. These difficulties include the large size of matrices required to describe excited states of complex atoms, the inherent numerical instability of algorithms that attempt to construct a principal representation from a given set of moments, and the difficulty of obtaining a meaningful continuous function $g(\epsilon)$ from a relatively sparse set of points ϵ_a in a principal representation. An additional problem arises in the description of resonance lines in the ionization continuum due to Rydberg series converging to low-lying positive-ion excited states. Relatively satisfactory solutions to these problems were found, involving new or modified procedures to be described below.

Section II of this paper reviews the theory and formalism used here. Section III describes the new or modified computational procedures proposed. Illustrative calculations on atomic He and B are reported in Secs. IV and V, respectively.

II. REVIEW OF THEORY

The frequency-dependent polarizability computed by standard bound-state methods is always of the form

$$\alpha(\omega)=\sum_i \frac{f_i}{\epsilon_i^2-\omega^2}. \tag{11}$$

The discrete excitation energies ϵ_i above the ionization threshold and the corresponding oscillator strengths f_i of Eq. (11) in general have no direct physical significance. Equation (11) represents $\alpha(\omega)$ above the ionization threshold as a real function with discrete poles. As more quadratically integrable basis states are included in a variational calculation, the density of poles increases, but $\alpha(\omega)$ remains qualitatively different from its correct limiting form, a complex function with smooth real and imaginary parts.

The Stieltjes imaging method proposed by Langhoff[1] bypasses this fundamental difficulty, using the mathematical theory of moments[6] to approximate the limiting complex function $\alpha(\omega)$. The directly computed excitation energies ϵ_i and oscillator strengths f_i are basis-set dependent and cannot be used directly as a valid principal representation of the physical oscillator-strength distribution. In practice, if there are N values of ϵ_i, a restricted set of moments is constructed, in the form

$$\mu_k=\sum_{i=1}^{N} f_i\,\epsilon_i^{-k}, \quad k=0,\ldots,2n-1, \tag{12}$$

where $n \ll N$. The computed values of these moments should converge to definite limits as variational calculations are improved, since the moments are, in principle, observable physical quantities. Principal representations with n pairs of values (ϵ_a, f_a) are constructed from the $2n$ moments, using various algorithms.[9] Each principal representation defines a cumulative oscillator-strength function $F(\epsilon)$ and its derivative $g(\epsilon)$, in the form of histograms given by Stieltjes imaging.[1] The use of the function $g(\epsilon)$ in extrapolating Rydberg-series oscillator strengths into the ionization continuum has been emphasized by Fano and Cooper.[7]

The most direct algorithm for constructing a principal representation from a given set of moments proceeds in two steps.[10] The first step is the construction of a symmetric tridiagonal matrix that will be defined below. This step is inherently numerically unstable. The second step, which is relatively free of numerical difficulties, is the diagonalization of this matrix. The eigenvalues are ϵ_a^{-1} and the eigenvectors determine the parameters f_a.

From Eqs. (3), (4), and (9),

$$\mu_k=\int_0^\infty g(\epsilon)\epsilon^{-k}\,d\epsilon \simeq \sum_a f_a\,\epsilon_a^{-k}. \tag{13}$$

Obviously the parameters (ϵ_a, f_a) have the significance of generalized Gaussian quadrature points and weights for the density function $g(\epsilon)$ over the interval $0 \leq \epsilon \leq \infty$. The mathematical theory of moments[6] and of generalized Gaussian quadrature is used to determine (ϵ_a, f_a) and then to reconstruct $g(\epsilon)$.

It is convenient to consider the general moment problem defined in terms of $x=\epsilon^{-1}$ by

$$\mu_k=\int_{x_1}^{x_2} \rho(x)x^k\,dx, \quad k=0,\ldots,2n-1, \tag{14}$$

where $\rho(x)$ is a non-negative density function. Such a density function defines a sequence of orthonormal polynomials $p_m(x)$, where m indicates the degree in x, such that

$$(p_m|p_{m'})=\int_{x_1}^{x_2} \rho(x)\,p_m(x)\,p_{m'}(x)dx=\delta_{mm'}, \tag{15}$$

in an obvious scalar product notation. It is well known that the Gaussian quadrature points ξ_a corresponding to Eqs. (14) are the roots of $p_n(x)$. For non-negative $\rho(x)$, these roots are real and lie in the interval $x_1 \leq \xi \leq x_2$. The orthonormal polynomials $p_m(x)$ satisfy recurrence relations of the form

$$xp_m = \beta_m p_{m-1} + \alpha_{m+1} p_m + \beta_{m+1} p_{m+1}, \quad m \geq 0, \tag{16}$$

with

$$p_{-1} \equiv 0, \quad p_0 = \beta_0^{-1} = \mu_0^{-1/2}, \tag{17}$$

so that

$$(p_0 | p_0) = \mu_0^{-1}\mu_0 = 1.$$

These recurrence relations, for $m \leq n$, can be expressed as a matrix equation,

$$\begin{bmatrix} \alpha_1 - x & \beta_1 & 0 & & \\ \beta_1 & \alpha_2 - x & \beta_2 & & \\ & \cdots & & & \\ & & & \beta_{n-1} & \alpha_n - x \end{bmatrix} \begin{bmatrix} p_0 \\ p_1 \\ \cdots \\ p_{n-1} \end{bmatrix} = \begin{bmatrix} 0 \\ 0 \\ \cdots \\ -\beta_n p_n \end{bmatrix}. \tag{18}$$

Since the inhomogeneous term here is proportional to $p_n(x)$, it vanishes at the roots of p_n, and the matrix in the left-hand member of Eq. (18) must be singular at these points. Hence the eigenvalues ξ_a $(a = 1, \ldots, n)$ of the symmetric tridiagonal matrix Ξ defined by the recurrence coefficients $(\beta_0, \alpha_1, \beta_1, \ldots, \alpha_n)$ are the roots of $p_n(x)$. The value of p_0 or β_0 indicated in Eq. (17) determines the normalization of the whole set of polynomials $p_m(x)$.

From Eqs. (16) it follows that Ξ is the matrix of the coordinate x in the linear space defined as in Eq. (15), with orthonormal basis $\{p_m\}$. Thus

$$\Xi_{mm'} = (p_m | x | p_{m'}) = \int_{x_1}^{x_2} \rho(x) p_m(x) x p_{m'}(x)\, dx. \tag{19}$$

Within the linear space of polynomials of degree less than n, a function $\varphi(x)$ has matrix elements

$$(p_m | \varphi(x) | p_{m'}) = [\underline{\varphi}(\Xi)]_{mm'} = \vec{e}_m \cdot \underline{\varphi}(\Xi) \cdot \vec{e}_{m'}, \tag{20}$$

where $\vec{e}_m$ is the unit vector corresponding to component p_m in Eq. (18). The function $\underline{\varphi}(\Xi)$ is defined as a matrix with the same eigenvectors as Ξ, with eigenvalues $\varphi(\xi_a)$. If the mth component of the normalized eigenvector $\vec{u}_a$ is denoted by u_{am}, Eq. (20) is equivalent to

$$(p_m | \varphi(x) | p_{m'}) = \sum_{a=1}^{n} u_{am} u_{am'} \varphi(\xi_a). \tag{21}$$

Since p_0 is a constant, equal to β_0^{-1}, Eq. (21) implies, for the moments defined by Eq. (14),

$$\mu_k = (\beta_0 p_0 | x^k | \beta_0 p_0) = \sum_a w_a \xi_a^k, \tag{22}$$

where

$$w_a = \beta_0^2 u_{a0}^2. \tag{23}$$

Equation (22) is a generalized Gaussian quadrature formula, valid for $k < 2n$. From Eq. (18),

$$u_{a0}^2 = p_0^2 \left(\sum_{m=0}^{n-1} p_m^2(\xi_a) \right)^{-1}, \tag{24}$$

so an alternative expression for the quadrature weights is

$$w_a = \left(\sum_{m=0}^{n-1} p_m^2(\xi_a) \right)^{-1}. \tag{25}$$

When applied to Eqs. (13), this theory gives

$$f_a = w_a, \quad \epsilon_a = \xi_a^{-1}, \tag{26}$$

for orthonormal polynomials $p_m(\epsilon^{-1})$.

In the theory of moments[6] the entire set of $2n$ moments is described by a function

$$I(z) = \int_{x_1}^{x_2} \frac{\rho(x)\, dx}{z - x} = \frac{\mu_0}{z} + \frac{\mu_1}{z^2} + \cdots + \frac{\mu_{2n-1}}{z^{2n}} + \cdots, \tag{27}$$

where z is a complex variable. This power-series representation of $I(z)$ can be converted to a continued fraction of the form

$$I_n(z) = \cfrac{\beta_0^2}{z - \alpha_1 - \cfrac{\beta_1^2}{z - \alpha_2 - \cdots - \cfrac{\beta_{n-1}^2}{z - \alpha_n}}}, \tag{28}$$

whose power-series expansion in z^{-1} reproduces the first $2n$ terms in Eq. (27). The coefficients $(\beta_0, \alpha_1, \ldots, \alpha_n)$ here are the same as those in Eqs. (16), the recurrence formulas for the orthogonal polynomials $p_m(x)$. This can be verified by generating the rational approximants of $I_n(z)$, since the successive denominators are polynomials proportional to the functions $p_m(z)$. From Eqs. (22), the first $2n$ terms of Eq. (27) are given exactly by the quadrature formula

$$I(z) \cong \sum_{a=1}^{n} \frac{w_a}{z - \xi_a}. \tag{29}$$

Several algorithms are available for computing the recurrence coefficients $(\beta_0, \alpha_1, \ldots, \alpha_n)$ from a given set of moments $(\mu_0, \ldots, \mu_{2n-1})$.[10-12] Whatever the form of the algorithm, this process is inherently numerically unstable.[11] It involves successive differencing of the given set of moments, and in practice is subject to very rapid loss of significant digits. It can be used to obtain generalized Gaussian quadrature formulas of high order only when exact analytic expressions are available for the moments μ_k. In contrast, the inverse process is highly stable,[11] since the moments can be expressed in terms of the recurrence coefficients $(\beta_0, \alpha_1, \ldots, \alpha_n)$ entirely as sums of positive numbers.

In order to avoid severe loss of numerical accuracy, it would be desirable to have a computational procedure that constructed these recurrence coefficients directly from the electronic Hamiltonian and dipole transition matrices. Such a procedure is described in Sec. III.

III. COMPUTATIONAL PROCEDURES

The configuration-interaction (electronic Hamiltonian) matrix required for a reasonably accurate description of the whole spectrum of excited states of a complex atom or molecule can be very large. Complete diagonalization of such a matrix can be prohibitively expensive. When the linear dimension N of this matrix is much greater than n, for a principal representation based on $2n$ moments μ_k, it is no longer efficient to use Eq. (12) to construct the moments. This formula requires complete diagonalization to determine the excitation energies ϵ_i and the corresponding eigenvectors of the configuration interaction matrix.

In the Appendix, the oscillator strengths appearing in Eqs. (11) and (12) are expressed in the form

$$f_i(ll) = C(L_0L_1)d_i(l)\epsilon_i d_i(l). \tag{30}$$

This is the dipole length-length formula. Length-velocity (lv) and velocity-velocity (vv) formulas are also given. The excitation energy

$$\epsilon_i = (h-\epsilon_0)_{ii} \tag{31}$$

is defined by an eigenvalue of the electronic Hamiltonian matrix h for states of total orbital angular momentum L_1. The computed energy of the ground state is ϵ_0 and its orbital angular momentum is L_0. The dipole-length transition matrix elements $0 \to i$ are denoted by $d_i(l)$. All states considered have the total spin S.

If the matrix h is not diagonalized, the oscillator strengths f_i in Eq. (12) must be replaced by a matrix version of Eq. (30). This results in

$$\mu_k(ll) = \sum_{L_1} C(L_0L_1) \times \sum_i \sum_j d_i(l)[(h-\epsilon_0)^{-k+1}]_{ij} d_j(l). \tag{32}$$

Similarly,

$$\mu_k(lv) = -\sum_{L_1} C(L_0L_1) \times \sum_i \sum_j d_i(l)[(h-\epsilon_0)^{-k}]_{ij} d_j(v), \tag{33}$$

$$\mu_k(vv) = \sum_{L_1} C(L_0L_1) \times \sum_i \sum_j d_i(v)[(h-\epsilon_0)^{-k-1}]_{ij} d_j(v). \tag{34}$$

These formulas avoid explicit diagonalization of the large matrix $h-\epsilon_0$. Inversion of this matrix would also be very inefficient. However, there is no need to obtain this inverse explicitly, since only contracted expressions of the form

$$\vec{d}^{\dagger} \cdot (h-\epsilon_0)^{-k}\vec{d} \tag{35}$$

are involved, where $\vec{d}$ is a vector. Such forms can be evaluated efficiently by use of triangular factorization,[13]

$$h - \epsilon_0 = t\sigma t^{\dagger}, \tag{36}$$

where t is a lower triangular matrix. The symbol "$\dagger$" here indicates the transpose of a real matrix. The matrix σ is diagonal, with elements ± 1. If $h-\epsilon_0$ is positive definite, as it is for excitations from the ground state, Eq. (36) reduces to Cholesky decomposition.[14] The more general form is retained here for eventual application to excited states. For $h-\epsilon_0$ factorized as in Eq. (36), evaluation of expressions such as Eq. (35) requires two processes involving large triangular matrices:

$$\vec{b}_1 = t^{-1}\vec{b}_0, \tag{37}$$

$$\vec{b}_2 = (t^{\dagger})^{-1}\sigma\vec{b}_1, \tag{38}$$

such that

$$\vec{b}_0 = \vec{d} \to \vec{b}_2 = (h-\epsilon_0)^{-1}\vec{d}. \tag{39}$$

An effective algorithm for Eq. (37) has been published previously.[13] A similar algorithm, including the data-handling procedures necessary to transpose a large triangular matrix, has been developed for Eq. (38), for use with the present method. By iteration of Eqs. (37) and (38), starting with $\vec{b}_0 = \vec{d}$, an expression of the form of Eq. (35) becomes a scalar product of the resulting vectors,

$$\vec{d}^{\dagger} \cdot (h-\epsilon_0)^{-k}\vec{d} = \begin{cases} \vec{b}_k^{\dagger} \cdot \sigma\vec{b}_k, & k \text{ odd}, \\ \vec{b}_k^{\dagger} \cdot \vec{b}_k, & k \text{ even}. \end{cases} \tag{40}$$

This technique was implemented in the present work for direct computation of μ_k in the three alternative versions (ll), (lv), and (vv) given by Eqs. (32)–(34).

Experience with this procedure indicates that moments μ_k can be generated very efficiently, but direct use of the resulting moments in the Stieltjes imaging method quickly runs into the severe numerical difficulties associated with construction of the recurrence coefficients $(\beta_0\alpha_1 \ldots \alpha_n)$ from the moments.

Sack and Donovan[15] have proposed an alternative method, based on modified moments

$$\nu_m = \int_{x_1}^{x_2} \rho(x) P_m(x)\, dx, \tag{41}$$

where the functions $P_m(x)$ are polynomials generated by specified recurrence formulas analogous to Eqs. (16). An algorithm is given[15] for converting this specified recurrence matrix into the corresponding matrix appropriate to the polynomials $p_m(x)$, orthogonal with respect to $\rho(x)$. By suitable choice of the polynomials $P_m(x)$, loss of numerical accuracy in this transformation can be greatly reduced in comparison with the original algorithm, which is equivalent to using pure monomials x^m for the functions $P_m(x)$.

In terms of the matrix Ξ defined by Eq. (19), the method of Sack and Donovan introduces a representation, in the basis of polynomials $P_m(x)$, intermediate between x^m and the final orthogonal polynomials $p_m(x)$. If the original data is a list of moments $\{\mu_k\}$, there can be no real numerical advantage in breaking the overall transformation into two steps. Thus the advantage gained in the transformation of modified moments $\{\nu_m\}$ to the final recurrence coefficients must be counteracted by numerical errors in transforming from the given moments $\{\mu_k\}$ to the modified moments.

For the applications considered here there is no way to obtain closed analytic expressions for modified moments. However, they could be constructed directly from the dipole transition vectors $\vec{d}$ and the electronic Hamiltonian matrix $h - \epsilon_0$ by suitable modification of Eqs. (32)–(34). It is possible to construct vectors of the form

$$P_m((h-\epsilon_0)^{-1})\vec{d} \tag{42}$$

which would satisfy the same recurrence relations as the polynomials $P_m(x)$, replacing x by the matrix $(h - \epsilon_0)^{-1}$. Then, from Eq. (32),

$$\nu_m(l\,l) = \sum_{L_1} C(L_0 L_1)\vec{d}(l) \cdot (h-\epsilon_0)\, P_m((h-\epsilon_0)^{-1})\vec{d}(l), \tag{43}$$

with similar expressions for $\nu_m(l\,v)$ and $\nu_m(vv)$.

The new method proposed here is to use Eqs. (42) and (43) to construct inductively the true orthonormal polynomials $p_m(x)$ and the associated sequence of recurrence coefficients. For these polynomials, the modified moments would be

$$\nu_m = \beta_0^2 \delta_{m0}. \tag{44}$$

Since these moments vanish except for $m = 0$, they are known to arbitrary accuracy. This method bypasses the construction of moments, thus avoiding the inherent numerical instability of the subsequent step from moments to recurrence coefficients.

Inductive formulas to generate the recurrence coefficients for the orthonormal polynomials $p_m(x)$ can be derived from the orthonormality conditions and from matrix elements of x. These formulas can then be used for vector functions of the matrix $(h - \epsilon_0)^{-1}$, as in Eq. (42). It is convenient to define the functions

$$\phi_m(x) = \beta_m p_m(x). \tag{45}$$

In terms of these functions, Eq. (16) implies

$$\phi_m = (x - \alpha_m)\beta_{m-1}^{-1}\phi_{m-1} - \beta_{m-1}\beta_{m-2}^{-1}\phi_{m-2}. \tag{46}$$

From matrix elements of this equation, for ϕ_{m+1},

$$\beta_m^2 = (\phi_{m-1}|x|\phi_m)\beta_{m-1}^{-1}, \tag{47}$$

$$\alpha_{m+1} = (\phi_m|x|\phi_m)\beta_m^{-2}. \tag{48}$$

The inductive process starts with

$$\begin{aligned} &\phi_{-2} \equiv 0, \quad \beta_{-2} \neq 0, \\ &\phi_{-1} = x^{-1}, \quad \beta_{-1} = 1, \quad \alpha_0 = 0. \end{aligned} \tag{49}$$

Then Eqs. (46)–(48) are used in sequence for $m = 0, \ldots, n-1$, omitting the last term in Eq. (46) when $m < 2$.

This process can be applied to vector functions as defined in Eqs. (42) and (43),

$$\begin{aligned} \vec{\phi}_m(l) &= \beta_m p_m((h-\epsilon_0)^{-1})\vec{d}(l), \\ \vec{\phi}_m(v) &= \beta_m p_m((h-\epsilon_0)^{-1})(h-\epsilon_0)^{-1}\vec{d}(v). \end{aligned} \tag{50}$$

Then, for a single value of L_1, matrix elements can be defined by

$$\begin{aligned} (\phi_m|x|\phi_{m'})_{ll} &= (\phi_m|(h-\epsilon_0)^{-1}|\phi_{m'})_{ll} \\ &= C(L_0L_1)\vec{\phi}_m(l)\cdot\vec{\phi}_{m'}(l), \\ (\phi_m|x|\phi_{m'})_{vv} &= (\phi_m|(h-\epsilon_0)^{-1}|\phi_{m'})_{vv} \\ &= C(L_0L_1)\vec{\phi}_m(v)\cdot\vec{\phi}_{m'}(v). \end{aligned} \tag{51}$$

The inductive equations (46)–(49) can be used with matrix elements of x or $(h - \epsilon_0)^{-1}$ defined in this way, and with ϕ_{-1} represented by

$$\vec{\phi}_{-1}(l) = (h-\epsilon_0)\vec{d}(l), \quad \vec{\phi}_{-1}(v) = \vec{d}(v). \tag{52}$$

It should be noted that the additional factor $h - \epsilon_0$ required in Eq. (32) and the factor $(h - \epsilon_0)^{-1}$ in Eq. (34) are included correctly in the formulas given above. The polynomials p_m and their recurrence coefficients differ in the two cases $(l\,l)$ and (vv), since the matrix elements of Eqs. (51) are not in general identical. The agreement between the $(l\,l)$ and (vv) results is a necessary (but not sufficient) criterion for the convergence of variational calculations. The mixed case $(l\,v)$ could also be considered, but has not been implemented in the present work because it would require two distinct vectors $\vec{\phi}_m(l)$ and $\vec{\phi}_m(v)$. For

both (ll) and (vv) cases, the inductive process requires retention of three vectors at any stage: $(h-\epsilon_0)^{-1}\vec{\phi}_m$, $\vec{\phi}_m$, and $\vec{\phi}_{m-1}$.

Since oscillator-strength distributions for different L_1 are independent, the Stieltjes imaging method can be applied separately for each L_1. This is done here. For electric dipole transitions $L_1 = L_0+1, L_0, L_0-1$, if $L_0>0$. If $L_0=0$, then $L_1=1$ only. When $L_0>0$, the three recurrence coefficient lists can be combined by use of an algorithm for adding continued fractions.[16] This has been implemented for the continued fractions defined by Eq. (28), yielding a combined recurrence coefficient list that reproduces the sums of the moments $\mu_k(L_1)$ for each k.

IV. ILLUSTRATIVE CALCULATIONS: HELIUM

In order to verify the theory outlined above and to test the computer programs written for this work, exploratory calculations were carried out for atomic helium and boron.

The calculations for He used a basis set of $7s$, $7p$, and $3d$ orbitals, with parameters listed in Table I. The exponents are taken from the matrix Hartree-Fock calculations of Clementi and Roetti, augmented and slightly modified to a geometric sequence,[17] extended until the first few computed moments of the oscillator-strength distribution had converged to reasonable values. For the ^1S ground state and the manifold of $^1P^o$ virtual excited states, all configurations that could be constructed from this orbital basis were included in the variational calculations. These are much less complete variational calculations than those of Langhoff *et al.*,[3] who used Hylleraas correlation factors, and of Rescigno *et al.*,[2] who report results with $12s$ and $8p$ orbitals. The basic calculation was very rapid, requiring 35 sec on an IBM 360/195 system. This work was not aimed at definitive results, but was intended only to provide an example of calculations at a level of accuracy that would be feasible for complex atoms.

TABLE I. He basis orbitals.

l	n	ζ
0	1	4.396 28
		2.496 03
		1.417 14
		0.804 59
		0.456 81
		0.259 36
		0.147 25
1	2	4.396 28
		2.496 03
		1.417 14
		0.804 59
		0.456 81
		0.259 36
		0.147 25
2	3	4.396 28
		2.496 03
		1.417 14

The main variational calculation is organized to proceed automatically from specification of the atom, quantum state, and basis-orbital parameters to produce the list of recurrence coefficients $(\beta_0 \cdots \alpha_n)$ defined by Eqs. (18) or (28). The results reported here were obtained with $n \leq 20$, although there appeared to be no difficulty in going to $n=30$ or more. Only (ll) results are given here, although (vv) results were also obtained and were used as a consistency check. The coefficient lists are very similar.

The principal representation obtained for He with $n=20$ is listed in Table II. For $n \geq 12$, exploratory calculations indicated that except at excitation energies greater than 2 Hartree units, the (ϵ, f) elements in the resulting principal representations did not vary significantly from those given here. This was also true for the alternative principal representations obtained with one value of ϵ set to $+\infty$.[9,10] Such representations were obtained in all cases considered here, but did not appear to provide any useful additional information.

Moments constructed from the principal representation of order 12 with no fixed point are listed in Table III. The first few even moments are compared with spectroscopic moments obtained by

TABLE II. He principal representation.

ϵ (e^2/a_0)	f
0.778 588	0.274 530
0.847 178	0.073 391
0.871 454	0.026 239
0.949 369	0.358 923
1.478 679	0.794 288
2.217 005	0.006 153
2.354 039	0.001 888
2.492 528	0.003 251
2.712 157	0.012 355
2.839 223	0.012 177
3.070 144	0.009 061
3.771 684	0.384 720
4.238 262	0.003 463
4.966 883	0.002 245
6.497 074	0.001 646
6.954 142	0.001 239
15.767 432	0.038 281
16.983 648	0.001 230
21.854 744	0.000 090
31.480 082	0.000 005

Leonard and Barker[18] from the best available theoretical and empirical data. The agreement is quite good, and is especially striking in view of the simple nature of the present calculations.

The constant coefficients in atomic or molecular interaction potentials (dispersion forces) that arise from induced electric dipole polarization can be expressed in terms of integrals over $\alpha(i\omega)$, where $\alpha(z)$ is the complex-valued polarizability.[19,20] From the Gaussian quadrature approximation provided by a principal representation, these integrals reduce to sums that can be evaluated in closed form.[21] In particular, the Van der Waals interaction constant is

$$C_6(A,B) \cong \frac{3}{2}\sum_a\sum_b \frac{f_{Aa}f_{Bb}}{\epsilon_{Aa}\epsilon_{Bb}(\epsilon_{Aa}+\epsilon_{Bb})}, \tag{53}$$

and the three-body dispersion-force coefficient is

$$\eta(A,B,C) \cong \frac{3}{2}\sum_a\sum_b\sum_c \frac{f_{Aa}f_{Bb}f_{Cc}(\epsilon_{Aa}+\epsilon_{Bb}+\epsilon_{Cc})}{\epsilon_{Aa}\epsilon_{Bb}\epsilon_{Cc}(\epsilon_{Aa}+\epsilon_{Bb})(\epsilon_{Bb}+\epsilon_{Cc})(\epsilon_{Cc}+\epsilon_{Aa})}. \tag{54}$$

The relativistic dispersion force is described by a potential proportional to R^{-4},[22] with coefficient

$$W_4 \cong \frac{1}{2}\sum_a\sum_b \frac{f_{Aa}f_{Bb}}{\epsilon_{Aa}+\epsilon_{Bb}}. \tag{55}$$

For interactions among ground-state He atoms, the present principal representation of order 12 gives, in Hartree atomic units,

$$C_6(\mathrm{He,He}) = 1.4654,$$
$$\eta(\mathrm{He,He,He}) = 1.4860, \tag{56}$$
$$W_4(\mathrm{He,He}) = 0.6656,$$

in comparison with the best available empirical or theoretical values,[18,22]

$$C_6(\mathrm{He,He}) = 1.4614,$$
$$\eta(\mathrm{He,He,He}) = 1.481, \tag{57}$$
$$W_4(\mathrm{He,He}) = 0.6643.$$

The agreement is excellent.

The cumulative oscillator-strength function $F(\epsilon)$ shown in Fig. 1 was constructed from the principal representation of order $n=20$ listed in Table II, using the Stieltjes imaging formula. The resulting function $F(\epsilon)$ is plotted against wavelength as the upper curve in Fig. 1. The conversion constant used here is[23]

$$\lambda(\text{Å}) \times \epsilon(e^2/a_0) = 455.6335. \tag{58}$$

The lower curve F in Fig. 1 is a cubic polynomial in ϵ^{-1} obtained by a least-squares fit to the function $F_I(\epsilon)$ defined by the six largest principal f values in Table II with $\epsilon<10.0$. This includes all elements (ϵ, f) of the principal representation with $\epsilon<2.0e^2/a_0$ ($\lambda>225$ Å), in the region of $(1snp)^1P^o$ excitations and the corresponding ionization continuum, and the single large f value with $\epsilon = 3.7717e^2/a_0$. For $\lambda<225$ Å, the remaining elements of the principal representation were used to define a function $\Delta F(\epsilon)$, fitted by a cubic natural spline curve[24] passing through the data points $\Delta F(\epsilon_a)$. The upper curve F in Fig. 1 is the sum of F_I and ΔF. The lower and upper curves σ_{PI} in Fig. 1 are obtained, respectively, from the derivatives of F_I and $F_I+\Delta F$, using Eq. (10). The upper curve σ_{PI} can be compared with the experi-

TABLE III. He moments (Hartree atomic units).

k	μ_k (calc)	μ_k (spect) [a]	k	μ_k (calc)
0	2.005 174 1	2.0000	12	6.882 753 9
1	1.507 448 2		13	8.606 372 5
2	1.384 994 2	1.3838	14	10.800 494
3	1.416 781 6		15	13.595 793
4	1.545 852 3	1.550	16	17.159 839
5	1.758 522 2		17	21.707 478
6	2.057 281 2	2.066	18	27.514 160
7	2.453 749 1		19	34.933 054
8	2.967 123 6	2.95	20	44.417 024
9	3.624 516 0		21	56.546 841
10	4.462 232 5		22	72.067 388
11	5.527 797 8		23	91.934 151

[a] Leonard and Barker, Ref. 18.

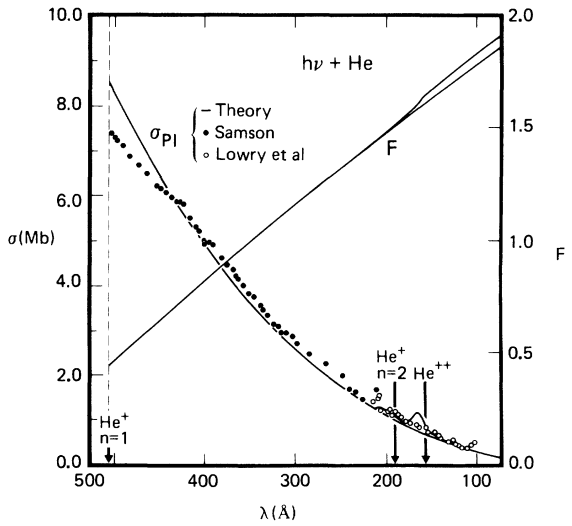

FIG. 1. He ground-state cumulative oscillator strength F and photoionization cross section σ_{PI}.

mental data of Samson,[25] for $\lambda > 209$ Å, and with that of Lowry *et al.*[26] for shorter wavelengths, as shown in Fig. 1. The agreement is good throughout this spectral region, although the present results rise above the experimental data by roughly 12% at threshold.

In constructing $F(\epsilon)$, the elements of the principal representation of Table II have been separated into two groups, treated as physically distinct contributions to the oscillator-strength distribution. This represents an attempt to distinguish between the one-electron excitations $(1skp)^1P^o$ and the Rydberg series and subsequent continua associated with $n=2$ and higher levels of He^+, culminating in the double-ionization states beyond $\lambda = 156.93$ Å. The $(1skp)^1P^o$ ionization continuum extends throughout the spectroscopic region considered here. In exploratory calculations, the large principal representation element at $3.7717e^2/a_0$ for $n=20$ in the present calculation was found to shift significantly in energy as the orbital basis set was changed. This behavior is uncharacteristic of a narrow resonance, and indicates that this (ϵ, f) element must be associated with the continuum. The very large oscillator strength of this element implies that it must belong to the series of singly excited states $(1skp)$, as do all $^1P^o$ states below $\epsilon = 2.0e^2/a_0$. The lower curves for F and σ_{PI} shown in Fig. 1 take only these elements of the principal representation into account, and are intended to represent the total effect of final states containing the $1s$ ground state of He^+.

The first accessible member of higher Rydberg series is the $(2s2p)^1P^o$ autoionizing state, observed[27] at $\lambda = 206.21$ Å. A direct calculation, with the orbital basis set used here, of the energy and oscillator strength for excitation of this state from the ground state gave

$$\epsilon = 60.328 \text{ eV} \quad (2.2170e^2/a_0),$$
$$f_l = 0.006\,15, \quad f_v = 0.006\,11, \tag{59}$$

compared with experimental values[27,18] of

$$\epsilon = 60.126 \text{ eV}, \quad f = 0.0048. \tag{60}$$

In Table II, the principal representation element at $2.2170e^2/a_0$ agrees with Eq. (59) to the number of significant digits shown. Apparently, the present calculations are capable of representing the lowest autoionizing states containing the first excited level of He^+ quite accurately. This justifies associating the principal representation elements with small f values found for ϵ between $2.0e^2/a_0$ and $3.7e^2/a_0$ (λ between 225 and 125 Å) with autoionizing states, as has been done here in constructing $\Delta F(\epsilon)$. The broad structure in σ_{PI} below the He^{++} threshold, apparent in Fig. 1, would then be attributed to the autoionizing states. This structure cannot be separated into individual resonance peaks without further information about their energy values and widths.

Spurious results would be obtained if oscillator-strength contributions from different excitation series were not separated as indicated above. In Table II, the six principal representation elements extending from $2.2170e^2/a_0$ to $3.0701e^2/a_0$, all with small f values, define a nearly horizontal segment of $F(\epsilon)$. If the large f value at $3.7717e^2/a_0$ is required to follow this sequence, the curve for $F(\epsilon)$ must rise abruptly, giving a large peak in $g(\epsilon)$ or σ_{PI} near $3.7717e^2/a_0$. Unless there is a physical resonance, this peak is spurious. Since this representation element appears to be the continuation of the $(1skp)^1P^o$ series, and since the element at $2.2170e^2/a_0$ is clearly identified with the $(2s2p)^1P^o$ autoionizing state, it is reasonable to separate the principal representation elements before constructing $F(\epsilon)$, as is done here. In effect, the rise in $F(\epsilon)$ due to the large f value at $3.7717e^2/a_0$ is assigned a width that overlaps the preceding (ϵ, f) elements, rather than being confined by an apparently unjustified assumption of no overlap.

In order to compute Van der Waals interaction constants, Dalgarno and Kingston[28] adjusted oscillator strengths for use in Eq. (53) so that Eqs. (4) would be satisfied in the form of sum rules for moments μ_k obtained from spectroscopic data. A refined version of this procedure was used by Leonard and Barker[18] to obtain the spectroscopic moments listed in Table III. The oscillator strengths obtained in this way for the $1\,^1S \rightarrow n^1P^o$ transition series are listed in Table IV.

TABLE IV. Reconstruction of $He(1snp)^1P^o$ Rydberg series.

n	λ(Å) [a]	f(calc)	f(spect) [b]
2	584.33	0.285 05	0.2762
3	537.03	0.078 50	0.0734
4	522.21	0.032 39	0.0309
5	515.62	0.016 50	0.0149
6	512.10	0.009 48	0.0085
7	510.00	0.005 98	0.0053
8	508.64	0.003 98	0.0036
9	507.72	0.002 81	0.0025
10	507.06	0.002 05	0.0018
11	506.57	0.001 55	
12	506.20	0.001 18	
13	505.91	0.000 92	
14	505.68	0.000 73	

[a] Martin, Ref. 29.
[b] Leonard and Barker, Ref. 18.

Since the Stieltjes imaging method constructs a continuous cumulative oscillator-strength function $F(\epsilon)$, this function can be interpolated[3,4] to define $F(\epsilon_i)$ at spectroscopic excitation energies.[29] Then the Stieltjes imaging formulas, Eqs. (6) and (7), can be used to reconstruct oscillator strengths f_i appropriate to the true spectroscopic transitions.[3,4] In effect, this is an application of the procedure of Dalgarno and Kingston.[28]

The working formula used here, given N values of $F(\epsilon_i)$, is

$$f_i + f_{i+1} = 2[F(\epsilon_{i+1}) - F(\epsilon_i)], \quad i = 1, \ldots, N-1. \tag{61}$$

This system of equations is singular. Any linear combination of particular solutions is also a solution if the weight coefficients add to unity. Each particular solution defines a parameter f_0 such that

$$f_0 + f_1 = 2F(\epsilon_1), \tag{62}$$

which completes the system of Eqs. (61). It is essential to choose f_0 so that both f_{N-1} and f_N are positive. In the present work, particular solutions are generated by choosing first $f_N = 0$, then $f_{N-1} = 0$, in both cases recurring backwards. Then $\{f_i\}$ is taken to be a weighted sum of these two solutions, chosen by the smoothing criterion that f_{N-2}, f_{N-1}, and f_N should define a linear function of ϵ_i.

Equations (61) and (62) imply that

$$\frac{f_0}{2} + \sum_{i=1}^{N-1} f_i + \frac{f_N}{2} = F(\epsilon_N). \tag{63}$$

When $f_0 \neq 0$, the solution is renormalized by multiplying each value f_i by the factor

$$F(\epsilon_N)/[F(\epsilon_N) - \tfrac{1}{2}f_0]. \tag{64}$$

This ensures that Eq. (63) holds for the final values of f_i, with $f_0 = 0$.

Oscillator strengths obtained in this way from the fitted function $F(\epsilon)$ of Fig. 1 are listed in Table IV. The present values are in good agreement with the best available values,[18] but tend to be systematically somewhat larger, consistent with the excess in σ_{PI} at threshold shown in Fig. 1. If the present function $F(\epsilon)$ is interpolated to the ionization threshold ($\lambda = 504.26$ Å), its value is 0.4461. The adjusted empirical sum of oscillator strengths[18] up to this threshold is 0.4258. The agreement is quite good.

As originally presented by Langhoff,[1] the Stieltjes imaging method would construct $F(\epsilon)$ as a piecewise linear function, whose derivative function $g(\epsilon)$ would be a histogram. This construction defines $F(\epsilon)$ as a spline function[24] of order 1. When enough data points are available to avoid interpolation over long intervals, it should be preferable to fit $F(\epsilon)$ by a cubic natural spline function.[24] Such a function has continuous first and second derivatives, with a piecewise linear second derivative. Hence $g(\epsilon)$ and its first derivative are continuous. A "natural" cubic spline function has zero second derivative at its end points, and hence is linear outside the range of defining points. It has the property of optimal smoothness for a cubic function, defined by minimizing the integral of the square of its second derivative over the range of data points.[24] This establishes an integral bound on the first derivative of $g(\epsilon)$ in the present case.

The curve $\Delta F(\epsilon)$ shown as the difference of the two curves $F(\epsilon)$ in Fig. 1, for $\lambda < 225$ Å, is a cubic natural spline function, defining $\Delta g(\epsilon)$ as shown. For $\lambda > 225$ Å, the data points were so sparse that the cubic spline function for $F_I(\epsilon)$ gave rather large oscillations in $g(\epsilon)$. In this region, a least-squares fit was used, as done in previous applications of this method.[3,5]

V. ILLUSTRATIVE CALCULATIONS: BORON

The calculations for B used a basis set of $6s$, $4p$, $2d$, and $1f$ orbitals, with parameters listed in Table V. The exponents are taken from the double-ζ basis of Clementi and Roetti, extended to a geometric sequence.[17] For the $(1s^2\,2s^2\,2p)^2P^o$ ground state and the manifold of ^2S, ^2P, and ^2D virtual excited states, all configurations representing one- or two-electron virtual excitations of the $2s^2\,2p$ shell that could be constructed from the orbital basis were included in the variational calculations. Results for oscillator strengths obtained for wave functions of this structure, but with larger orbital basis sets, have recently been

TABLE V. B basis orbitals.

l	n	ζ
0	1	6.566 57
		4.249 27
	2	1.413 14
		0.875 64
		2.280 58
		0.542 58
1	2	2.217 34
		1.005 51
		4.889 65
		0.455 97
2	3	2.217 34
		1.005 51
3	4	2.217 34

reported for the resonance transitions of ions of the Be I isoelectronic sequence.[30] The computed dipole-length oscillator strengths appear to be of quite good accuracy.

Boron is the simplest atom with $L>0$ in its ground state. The three resulting virtual excitation manifolds of the ground state were computed separately, to give the principal representations of the oscillator-strength distributions listed in Table VI. For comparison with experimental data, these f values have all been renormalized by a common factor to make their sum exactly 3.0. The sum of directly computed f values was 3.1519. The basic calculation required only 80 sec on an IBM 360/195 system.

Also listed in Table VI is the total principal representation of order $n=15$ obtained by summing[16] the continued fractions defined by Eq. (28) for the ^2S, ^2P, and ^2D excitation manifolds. The first 30 moments $\mu_0 \cdots \mu_{29}$ determined by this representation are each the sum of the corresponding moments for the individual excitation manifolds.

The value of μ_2 (total) determined by the present calculation is $18.1585a_0^3$. This is the static polarizability. This computed value, equal to 2.69 Å^3, is in good agreement with recent theoretical results, 2.85 Å^3 (Stevens and Billingsley[31]) and 2.93 Å^3 (Mukherjee *et al.*[32]).

The Stieltjes imaging method for constructing the photoionization cross section from a given principal representation can produce qualitatively incorrect results if the excitation spectrum is a superposition of weakly interacting component spectra. In the case of He, discussed above, it was necessary before constructing $F(\epsilon)$ and $g(\epsilon)$ to separate principal representation elements (ϵ_a, f_a) associated with the ground state of He^+ from the much weaker elements associated with excited states of He^+. The essential problem is that Eqs. (6) and (7) of the Stieltjes imaging method confine the full effect of any f_a to the interval between the adjacent energy values ϵ_{a-1} and ϵ_{a+1}. When the principal representation elements are relatively sparse, one large f_a value may represent the integrated effect of a smooth excitation curve extended over a broad enery range. If physically distinct excitations (such as the autoionizing states of He, superimposed on the $1skp$ excitation continuum) produce other principal representation elements within this energy range, the large element (ϵ_a, f_a) would appear as a large but spurious peak, confined between the neighboring representation elements arising from distinct excitation processes.

This aspect of the Stieltjes imaging method presents serious difficulties for applications to complex atoms. In the case of He, the excitation series associated with $He^+(1s)$ could be separated from the full representation because all large oscillator-strength elements could be assumed to be in this series. For complex atoms, the various positive-ion states may produce several relatively strong excitation series, which must be disentangled before qualitatively correct curves can be obtained for $F(\epsilon)$ or $g(\epsilon)$. This requires careful consideration of the structure of the possible excitation manifolds and identification of weak resonances superimposed on stronger continuum excitation backgrounds. An analysis of the boron ground-state excitation spectrum is given here as an example of the reasoning that might be applied.

Stieltjes image data points for $F(\epsilon)$ defined by

TABLE VI. B principal representations (ϵ in e^2/a_0).

^2S		^2P		^2D		Total	
ϵ	f	ϵ	f	ϵ	f	ϵ	f
0.184 122	0.079 321	0.334 122	0.568 152	0.220 554	0.077 569	0.184 122	0.079 321
0.293 900	0.074 665	0.409 468	0.039 705	0.392 830	0.900 929	0.220 554	0.077 569
0.397 900	0.040 028	0.577 508	0.000 109	0.434 852	0.265 540	0.293 900	0.074 665
0.454 644	0.000 180	0.665 256	0.003 015	0.569 109	0.000 592	0.334 122	0.568 156
0.584 801	0.001 329	0.828 092	0.005 162	0.669 561	0.002 492	0.392 970	0.938 650
0.747 114	0.000 356	0.873 482	0.061 521	0.871 498	0.025 687	0.412 991	0.052 499
0.881 760	0.005 473	0.984 253	0.003 023	0.909 534	0.048 854	0.435 351	0.255 370
0.996 123	0.011 407	1.127 848	0.054 310	1.123 328	0.053 218	0.621 137	0.005 481
1.172 385	0.015 600	1.349 968	0.058 475	1.240 585	0.175 447	0.855 364	0.102 585
1.292 530	0.026 668	1.580 083	0.003 750	1.799 634	0.096 270	1.000 576	0.116 598
2.095 541	0.006 159	2.426 085	0.010 034	1.964 637	0.068 981	1.253 043	0.329 271
2.483 550	0.004 848	3.293 280	0.001 728	2.585 232	0.013 691	1.879 719	0.178 370
3.883 295	0.000 617	4.860 680	0.000 519	4.177 930	0.001 443	2.724 315	0.027 451
9.580 985	0.021 522	9.588 166	0.062 951	9.572 919	0.104 691	9.532 640	0.189 136
25.104 812	0.001 172	25.357 702	0.001 418	25.512 670	0.001 379	23.239 120	0.004 878

Eqs. (6) and (7) for the total principal representation listed in Table VI were fitted by a cubic natural spline function.[24] The resulting curves for $F(\lambda)$ and σ_{PI} [from the derivative function $g(\epsilon)$] are shown in Fig. 2 for energies above the known line spectra of B I; σ_{PI} is plotted only above the $(2s2p)^1P^o$ threshold of B II at 712.6 Å ($\epsilon = 0.639\,40 e^2/a_0$). Line spectra are observed at longer wavelengths, superimposed on an ionization continuum between the $(2s2p)^3P^o$ threshold at 960 Å ($0.475\,11 e^2/a_0$) and the $(2s^2)^1S$ threshold at 1494.1 Å ($0.304\,96 e^2/a_0$). Reconstruction of the intensity distributions in these line spectra will be discussed below.

Preliminary results of electron scattering calculations of the atomic boron photoionization cross section[33] indicate that σ_{PI} is a decreasing function of energy above the $^1P^o$ threshold. This suggests that the peak shown in Fig. 2 is a computational artifact, due to failure to separate physically distinct contributions to the excitation spectrum. The obvious separation into ^2S, ^2P, and ^2D components changes the total σ_{PI} curve, but does not eliminate what appears to be spurious structure. In order to examine this question more closely, the ^2D excitation spectrum, which accounts for more than half of the total oscillator strength for valence-shell excitations, will be analyzed here in detail. With certain plausible assumptions, it turns out to be possible to subdivide this excitation spectrum so that the reconstructed photoionization cross section is physically reasonable.

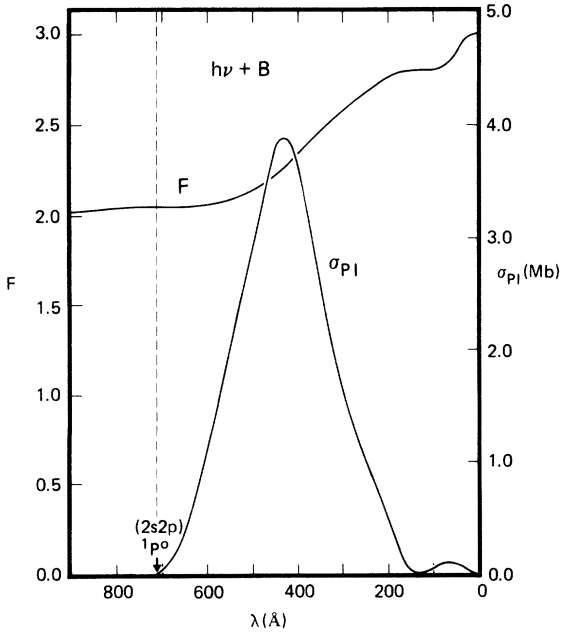

FIG. 2. B F and σ_{PI} from Stieltjes imaging of total principal representation.

The Rydberg series of excitations of the $(2s^22p)^2P^o$ ground state of B I that converge to the $(2s^2)^1S$ ground state of B II are of the form $(2s^2ns)^2S$ and $(2s^2nd)^2D$. The only other electric-dipole-allowed transitions in this energy range are to the ^2S and ^2D states of configuration $(2s2p^2)$.

From its energy value, the first ^2D principal representation element in Table VI primarily describes the $(2s2p^2)^2D$ excitation line. Since only ^2D states can arise from coupling nd orbitals to the $(2s^2)^1S$ state of B II, the oscillator strength due to $2p \rightarrow nd$ transitions (or $2p \rightarrow kd$ in the continuum) is confined to the ^2D excitations. In the present calculations, this oscillator strength is concentrated in the second ^2D principal representation element in Table VI. This was verified by repeating the calculations with all d orbitals removed, which eliminated this principal representation element.

The oscillator strengths of the observed $^2P^o \rightarrow {}^2D$ lines below the $(2s^2)^1S$ threshold of B II were reconstructed from a polynomial defined to fit the cumulative oscillator-strength function for the first two ^2D elements of Table VI:

$$F_1 = 0.978\,498 - 0.138\,163\epsilon^{-1} - 0.015\,239\epsilon^{-2}. \tag{65}$$

The curve $F_1(\epsilon)$ passes through the two data points at ϵ_1 and ϵ_2, defined by Eq. (7) in this case, and also through the implied point at infinity, preserving the sum $f_1 + f_2$. $F_1(\epsilon)$ vanishes at $\epsilon = 0.213\,98$, below the first ^2D state of B I.

Oscillator strengths were determined at experimental excitation energies[34,35] following the procedure described in Sec. IV. The lowest ^2D state is of configuration $2s2p^2$, which distinguishes it from the $2s^2nd$ Rydberg series. Hence the first $^2P^o \rightarrow {}^2D$ oscillator strength was taken to be exactly twice the local value of $F(\epsilon)$, in accord with Eq. (62) when $f_0 = 0$. The subsequent f values, for the $2s^2nd$ series, were renormalized by the common factor defined by Eq. (64). These reconstructed oscillator strengths are listed in Table VII. Experimental oscillator strengths[36-40] are known only for the first two $^2P^o \rightarrow {}^2D$ transitions. The present results fall within the range of these experimental values.

Absorption lines of a second ^2D Rydberg series, converging to the $(2s2p)^3P^o$ state of B II, have been observed.[35] These lines are broadened by autoionization, since they lie above the B II ground state. The upper states of these transitions are assumed to be of the form $(2s2p)^3P^o np$, arising from $2s \rightarrow np$ transitions. In the present calculations, the discrete part of this transition series must be associated with the ^2D principal representation element at $\epsilon = 0.4349$ (1048 Å), between

TABLE VII. Reconstruction of B ^2D Rydberg series.

State	λ(Å) [a,b]	f(calc)	f(obs)
$2s2p^2$	2089.6	0.048 71	0.059,[c] 0.048,[d] 0.050,[e] 0.054,[f] 0.045 [g]
$2s^2 3d$	1826.0	0.166 30	0.175,[d] 0.15,[e] 0.19,[f] 0.20 [g]
4	1667.0	0.061 14	
5	1600.5	0.031 11	
6	1566.2	0.015 90	
7	1546.5	0.010 84	
8	1533.9	0.006 21	
9	1525.6	0.005 01	
10	1519.7	0.003 07	
11	1515.5	0.002 42	
12	1512.3	0.001 92	
13	1509.7	0.001 51	
$2s2p3p$	1141.7	0.100 34	
4	1044.8	0.031 80	
5	1009.8	0.014 56	
6	992.5	0.008 14	
7	982.8	0.004 48	

[a] Moore, Ref. 34.
[b] Esteva, Ref. 35.
[c] Bergström *et al.*, Ref. 36.
[d] Lawrence and Savage, Ref. 37.
[e] Bromander, Ref. 38.
[f] Smith and Wiese, Ref. 39.
[g] Kernahan *et al.*, Ref. 40.

the ^1S and $^3P^o$ thresholds of B II. Since this large contribution to the cumulative oscillator strength should extend into the ionization continuum above the $^3P^o$ threshold, it must be associated with at least one large principal representation element at higher energy. In Table VI, the largest ^2D f value at higher energy occurs at $\epsilon = 1.2406$. The quadratic polynomial in ϵ^{-1} defined by these two principal representation elements, fitted as in the definition of Eq. (65), is

$$F_2 = 0.440\,987 - 0.095\,227\epsilon^{-1} - 0.016\,873\epsilon^{-2}. \tag{66}$$

$F_2(\epsilon)$ vanishes at $\epsilon = 0.331\,40$, above the ^1S threshold of B II but below the first observed line $(2s2p3p)^2D$ of this excitation series. This is consistent with use of F_2 to represent the cumulative oscillator strength of this series. The coefficient of ϵ^{-2} in F_2 is consistent in magnitude with the quadratic term in F_1, given by Eq. (65).

Oscillator strengths for the $(2s2pnp)^2D$ series constructed from $F_2(\epsilon)$ at the experimental excitation energies[35] are listed in Table VII. No experimental oscillator strengths are available, but the present values are consistent with observation of a rather strong series of absorption lines.[35]

This reconstructed line spectrum, together with the continuous functions F_1 and F_2, defines the cumulative oscillator-strength function $F(\epsilon)$ shown in Fig. 3. Absorption lines appear as vertical steps. Above the $(2s^2)^1S$ state of B II, $g_1(\epsilon)$, the derivative of $F_1(\epsilon)$, provides a continuum absorption background to the line spectrum. The line spectrum converging to the B II $(2s2p)^3P^o$ threshold is continued above this threshold by $g_2(\epsilon)$, which gives the function $g(\epsilon)$ shown in Fig. 3 when added to $g_1(\epsilon)$. No Rydberg series converging to the B II $(2s2p)^1P^o$ threshold have been observed. This is consistent with the present calculations, since the ^2D principal representation contains only one very small element between the $^3P^o$ and $^1P^o$

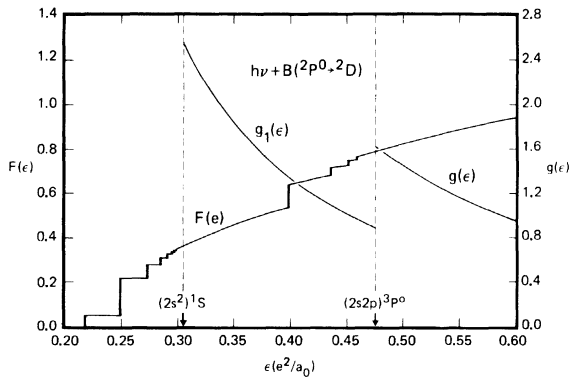

FIG. 3. B ground-state ^2D component of cumulative oscillator strength F and oscillator-strength distribution g.

thresholds ($f = 0.0006$ at $\epsilon = 0.5691$). This oscillator strength is too small to be visible on the scale of Fig. 3.

The total photoionization cross section shown in Fig. 2 nearly vanishes at the $(2s2p)^1P^o$ threshold of B II. In contrast, the function $g(\epsilon)$ shown in Fig. 3, a monotonically decreasing function, gives $\sigma_{PI} = 3.2937$ Mb from ^2D excitations alone at the $^1P^o$ threshold (712.6 Å or $0.6394e^2/a_0$). A large part of the broad peak in σ_{PI} shown in Fig. 2 must be distributed over a wider energy range in order to be compatible with the indicated reconstruction of observed line spectra.

Although no line spectra have been observed beyond the $(2s2p)^3P^o$ threshold, Rydberg series of excitation resonances may be formed by electron attachment to excited B II states of configuration $2p^2$. The $(2s^22p)^2P^o$ ground state of B I gains a relatively large component of structure $(2p^3)^2P^o$ by configuration interaction. Transitions to states of structure $2p^2ns$ or $2p^2nd$ may have substantial oscillator strength due to one-electron transitions $2p \rightarrow ns$ or $2p \rightarrow nd$ from the $(2p^3)^2P^o$ component of the ground state. This could give rise to several distinct excitation series at energies above the $(2s2p)^1P^o$ threshold, with final ^2D states of structure $(2p^2)^3Pnd$, $(2p^2)^1D(ns, nd)$, and $(2p^2)^1Snd$.

In the absence of experimental data and of more detailed calculations, no definite conclusions can be drawn about these higher excitation series, although wave functions of this structure are contained in the calculations presented here. In fact, it was found that three additional pairs of elements in the ^2D principal representation listed in Table VI could be fitted to polynomials similar to F_1 and F_2, with small quadratic terms in ϵ^{-1}. The additional three polynomials are

$$F_3 = 0.055\,710 - 0.020\,187\epsilon^{-1} - 0.010\,901\epsilon^{-2}, \tag{67}$$

from the ^2D principal representation elements at $\epsilon = 0.6696$ and $\epsilon = 1.1233$;

$$F_4 = 0.117\,835 - 0.052\,936\epsilon^{-1} - 0.029\,125\epsilon^{-2}, \tag{68}$$

from the elements at $\epsilon = 0.9095$ and 1.9646; and

$$F_5 = 0.121\,957 - 0.078\,675\epsilon^{-1} - 0.014\,307\epsilon^{-2}, \tag{69}$$

from the elements at $\epsilon = 0.8715$ and 1.7996. The functions F_3, F_4, and F_5 vanish at $\epsilon = 0.659\,20$, 0.770 17, and 0.793 04, respectively. This is compatible with excitation series of resonances above the $(2s2p)^1P^o$ threshold at $\epsilon = 0.639\,40e^2/a_0$ ($\lambda = 712.6$ Å). The functions F_3, F_4, and F_5 are defined only for ϵ greater than the points at which they vanish.

To illustrate the effect of separating distinct excitation series, Fig. 4 shows the cumulative oscillator-strength function $F(\epsilon)$ for ^2D excitations, expressed as the sum of $F_1, \ldots, F_5$ and of a cubic spline function defined by the remaining ^2D principal representation elements from Table VI. The ^2D photoionization cross section σ_{PI} shown in Fig. 4 is obtained from the sum of derivative functions $g_1, \ldots, g_5$ and of the derivative of the residual spline function. If line spectra corresponding to these assumed excitation series were known, the initial part of each function F_i would be replaced by a histogram, as in Fig. 3, and each function g_i would commence with a series of δ functions, eventually merging into the continuous functions approximated here. Since autoionizing states are involved, the discrete part of g_i would actually be a series of resonance profile structures. In the absence of information on resonance line positions and widths, each function g_i is presented here as a smooth function, discontinuous at its origin (where F_i vanishes). These discontinuities appear prominently in Fig. 4.

The $^2P^o \rightarrow {}^2P$ excitation spectrum is dominated by a single strong line, for the upper state $(2s2p^2)^2P$ at $\lambda = 1378.5$ Å or $\epsilon = 0.33053e^2/a_0$. This line must be associated with the ^2P principal representation element ($\epsilon = 0.3341$, $f = 0.5682$) in Table VI. Smith and Wiese[39] give $f = 0.58$ for this line. A recently observed value[40] is $f = 0.63 \pm 0.06$.

Oscillator strengths of the observed $^2P^o \rightarrow {}^2S$ lines below the $(2s^2)^1S$ threshold of B II were reconstructed from a polynomial in ϵ^{-1}. This polynomial was fitted to the first three Stieltjes data

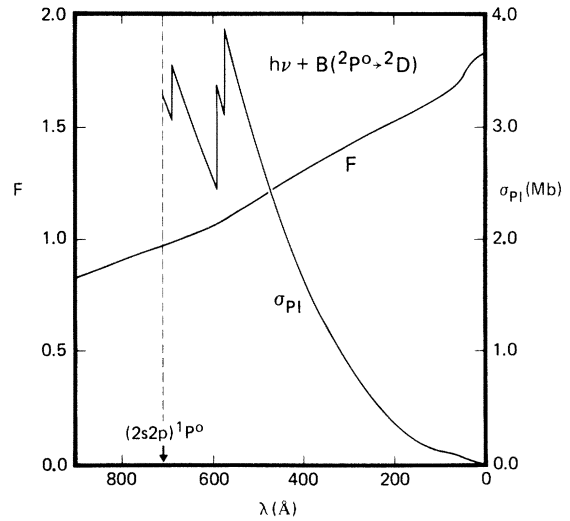

FIG. 4. B ground-state ^2D component of F and σ_{PI}, from separated excitation series.

points of the histogram for $F(\epsilon)$ constructed from the ^2S principal representation listed in Table VI. This polynomial is

$$F = 0.413\,805 - 0.118\,268\epsilon^{-1} + 0.009\,092\epsilon^{-2}. \quad (70)$$

Oscillator strengths determined at the experimental excitation energies[34,35] are listed in Table VIII. Experimental oscillator strengths,[36,38-40] known only for the first line in the series, bracket the present value. The $(2s2p^2)^2S$ state occurs between $n = 6$ and 7 in the $(2s^2ns)^2S$ series. Since line strengths are not computed individually in the present work, their values are determined from the smooth curve for $F(\epsilon)$ entirely by the energy intervals of neighboring lines. This construction assigns a relatively large oscillator strength to the $2s2p^2$. Qualitative line-intensity observations[34] indicate that these relative intensities should be reversed. It would be possible to resolve this point by direct computation of the oscillator strength for excitation to $(2s2p^2)^2S$ in a variational calculation that could represent explicit ns orbitals for the neighboring Rydberg states.

VI. DISCUSSION

The present paper has considered three main aspects of the practical application of the Stieltjes imaging method of Langhoff.[1] The first aspect is the technical problem of obtaining a numerically valid principal representation of the oscillator-strength distribution for excitations from the ground state of a complex atom. This appears to be dealt with adequately through the revised algorithms presented in Sec. III. The most important practical development in computational procedure introduced here is the direct construction of the recurrence coefficients $(\beta_0, \ldots, \alpha_n)$ of Eqs. (18) and (28), since this bypasses the numerically unstable step in the usual method of moments. It has been shown here that this revised method retains sufficient detail in the excitation spectrum to describe the $(2s2p)^1P^o$ autoionizing state of He, whose quite small oscillator strength is superimposed on the much larger absorption continuum of the $(1skp)^1P^o$ excitation series.

The second aspect of this general method considered here is the direct use of a principal representation to compute Van der Waals coefficients and to reconstruct oscillator strengths for line spectra at observed energy values. Results obtained for He and B, based on exploratory calculations that are very inexpensive in computer time, are in good agreement with all available quantitative data for the ground states of these atoms and for their excitation spectra. This use of the present method opens up a rich field for possible applications, unifying the quantitative treatment of ground-state excitation spectra over the full range of observed energies. The prospect of rapid and accurate computation of Van der Waals constants and related quantities may be of considerable importance in the quantitative study of interatomic and intermolecular forces.

The third aspect considered here, the construction of the photoionization cross section from principal representation data on the oscillator-strength distribution, suffers from difficulties inherent in the physics of complex atoms. When several low-lying states of the detached species exist, several distinct excitation series of comparable intensity may contribute to the excitation spectrum. As shown here, it is necessary to separate a given principal representation of the oscillator-strength distribution into the individual

TABLE VIII. Reconstruction of B ^2S Rydberg series.

State	λ(Å) [a,b]	f(calc)	f(obs)
$2s^2 3s$	2497.5	0.069 49	0.055,[c] 0.090,[d] 0.062,[e] 0.087 [f]
4	1817.9	0.031 40	
5	1662.6	0.003 84	
6	1610.4	0.008 89	
$2s2p^2$	1573.3	0.000 44	
$2s^2 7s$	1558.7	0.003 31	
8	1539.8	0.001 59	
9	1529.6	0.001 09	
10	1522.5	0.000 78	
11	1517.4	0.000 57	
12	1513.7	0.000 42	

[a] Moore, Ref. 34.
[b] Esteva, Ref. 35.
[c] Bergström *et al.*, Ref. 36.
[d] Bromander, Ref. 38.
[e] Smith and Wiese, Ref. 39.
[f] Kernahan *et al.*, Ref. 40.

contributions of such excitation series before the photoionization cross section can be obtained without spurious large-scale structure. This means that a careful analysis of observed line spectra and absorption resonance series and construction of the cumulative oscillator-strength functions that continue such series into the photoionization continuum is an essential step in the practical use of the Stieltjes imaging method.

Two important extensions of the present method have not been discussed here. The first is implementation for molecules. It is clear that this presents no serious practical difficulty, given the technical developments of the method described here. For molecules, it will be important to consider electric quadrupole and octupole excitations, so that higher Van der Waals coefficients can be computed.

The second major extension of this method is to the excitations of excited states, including inner-shell vacancy states. For this purpose, it will be necessary to modify the algorithms given here so that negative oscillator strengths may be considered. This development does not appear to present any essential difficulty.

In summary, the method considered here provides a powerful unifying formalism for the quantitative study of the intensity distributions in atomic and molecular spectra, including continuations of line spectra or resonance series into the photoionization or photodetachment continuum. Preliminary results indicate that quantitative data can be obtained with relative ease for a wide range of possible applications.

ACKNOWLEDGMENTS

The author is indebted to J. T. Broad, W. P. Reinhardt, S. O'Neill, M. LeDourneuf, and Vo Ky Lan for communication of unpublished results of theoretical calculations; to the CNRS for partial support of a visit to the Observatoire de Paris, Meudon, where this work was initiated; to the National Science Foundation for a travel grant; to H. van Regemorter for the hospitality of his research group during this visit; and especially to W. P. Reinhardt for several very helpful discussions to the technical subtleties of this work.

APPENDIX: COMPUTATION OF ATOMIC OSCILLATOR STRENGTHS

Consider an electric dipole transition from electronic state 0 to state i, both described by variational wave functions. The orbital angular momentum quantum numbers are L_0, M_0; L_i, M_i. The dipole-length formula for the oscillator strength is

$$f_i = \frac{2}{3}\frac{(E_i - E_0)}{(2L_0+1)}\sum_{M_0}\sum_{M_i}\frac{(0|\vec{r}|i)\cdot(i|\vec{r}|0)}{(0|0)(i|i)} \tag{A1}$$

$$= \frac{2}{3}\frac{E_i - E_0}{(2L_0+1)(0|0)(i|i)}(i\|\vec{r}\|0)^2, \tag{A2}$$

where $(i\|\vec{r}\|0)$ is a reduced matrix element[41] of the electronic operator

$$\sum_{a=1}^{N}\vec{r}_a . \tag{A3}$$

The reduced matrix element $(i\|\vec{r}\|0)$ is a real number, with

$$(i\|\vec{r}\|0) = (-1)^{L_0 - L_i}(0\|\vec{r}\|i). \tag{A4}$$

In the present work, a variational wave function for an N-electron atom is expressed as a linear combination of LS eigenfunctions. These are constructed for each electronic configuration as explicit linear combinations of Slater determinants. An algorithm[42] is used that produces a standard state with $M_L = L$, $M_S = S$. Matrix elements of operators such as Eq. (A3) between such functions are computed using simple general formulas valid for Slater determinants.[43] For such standard LS states the definition of reduced matrix elements[41] gives

$$(i|\vec{r}|0)_{\text{stand}} = \begin{pmatrix} L_i & 1 & L_0 \\ -L_i & L_i - L_0 & L_0 \end{pmatrix}(i\|\vec{r}\|0). \tag{A5}$$

Then Eq. (A2) can be expressed in the form

$$f_i(ll) = C(L_0L_i)d_i(l)\epsilon_i d_i(l), \tag{A6}$$

where

$$C(L_0L_i) = \tfrac{2}{3}(0|0)^{-1}(2L_0+1)^{-1} \times \begin{pmatrix} L_i & 1 & L_0 \\ -L_i & L_i - L_0 & L_0 \end{pmatrix}^{-2}, \tag{A7}$$

$$d_i(l) = (i|i)^{-1/2}(i|\vec{r}|0)_{\text{stand}},$$

$$\epsilon_i = E_i - E_0.$$

The 3-j symbol in $C(L_0L_i)$ can be evaluated[41] to give

$$\frac{1}{2L_0+1}\begin{pmatrix} L_i & 1 & L_0 \\ -L_i & L_i - L_0 & L_0 \end{pmatrix}^{-2} = \begin{cases} 1, & L_i = L_0 - 1, \\ (L_0+1)/L_0, & L_i = L_0, \\ (2L_0+3)/(2L_0+1), & L_i = L_0 + 1. \end{cases} \tag{A8}$$

Equation (A6) is the length-length (ll) form of the oscillator strength. Alternative formulas can

be expressed in terms of dipole-velocity and dipole-acceleration matrix elements, given respectively by

$$d_i(v) = (i\,|\,i)^{-1/2}(i\,|\,\vec{\nabla}|\,0)_{\text{stand}},$$
$$d_i(a) = (i\,|\,i)^{-1/2}(i\,|\,Zr^{-3}\vec{r}\,|\,0)_{\text{stand}}, \tag{A9}$$

where Ze is the nuclear charge. For complex atoms the most useful formulas, in addition to $f_i(ll)$ of Eq. (A6), are the length-velocity (lv) and velocity-velocity (vv) expressions, respectively,

$$f_i(lv) = -C(L_0L_i)d_i(l)d_i(v), \tag{A10}$$

$$f_i(vv) = C(L_0L_i)d_i(v)\epsilon_i^{-1}d_i(v). \tag{A11}$$

The algorithms mentioned above reduce all transition matrix elements to linear combinations of integrals between orthonormal one-electron orbital functions. The angular factors (denoted by subscript Ω) of these matrix elements can all be expressed in terms of the integrals

$$(l+1, m|\, r_{m-m'}|\, l, m')_\Omega = c^1(l+1, m; l, m')r,$$
$$(l+1, m|\, \nabla_{m-m'}|\, l, m')_\Omega = c^1(l+1, m; l, m')\left(\frac{\partial}{\partial r} - \frac{l}{r}\right), \tag{A12}$$
$$(l+1, m|\, Zr^{-3}r_{m-m'})_\Omega = c^1(l+1, m; l, m')Zr^{-2},$$

where the coefficients $c^1(l+1; l)$ are Gaunt coefficients tabulated by Condon and Shortley.[43] The matrix element of $\vec{\nabla}$ is anti-Hermitian, and the others are Hermitian.

This formalism has been used for recent accurate calculations of oscillator strengths for the Be I isoelectronic sequence.[30]

---

*Supported in part by the Office of Naval Research, Contract No. N00014-72-0051.

[1]P. W. Langhoff, Chem. Phys. Lett. 22, 60 (1973).
[2]T. N. Rescigno, C. W. McCurdy, Jr., and V. McKoy, Phys. Rev. A 9, 2409 (1974).
[3]P. W. Langhoff, J. Sims, and C. T. Corcoran, Phys. Rev. A 10, 829 (1974).
[4]P. W. Langhoff and C. T. Corcoran, J. Chem. Phys. 61, 146 (1974).
[5]J. T. Broad and W. P. Reinhardt, in *Electronic and Atomic Collisions, Abstracts of the Papers of the Ninth International Conference on the Physics of Electronics and Atomic Collisions,* edited by J. S. Risley and R. Geballe (Univ. of Washington Press, Seattle, 1975), p. 381; Chem. Phys. Lett. 37, 212 (1976).
[6]J. A. Shohat and J. D. Tamarkin, *The Problem of Moments, Mathematical Surveys 1* (American Mathematical Society, Providence, 1943).
[7]U. Fano and J. W. Cooper, Rev. Mod. Phys. 40, 441 (1968).
[8]T. Stieltjes, Ann. Fac. Sci. Univ. (Toulouse) 8, J1 (1894); 9, A1 (1894).
[9]J. C. Wheeler and R. G. Gordon, in *The Padé Approximant in Theoretical Physics,* edited by G. A. Baker, Jr., and J. L. Gammel (Academic, New York, 1970), pp. 99–128.
[10]R. G. Gordon, J. Math. Phys. 9, 655 (1968).
[11]H. Rutishauser, *Der Quotienten-Differenzen-Algorithmus* (Birkhäuser, Basel, 1957); P. Henrici, Proc. Symp. Appl. Math. 15, 159 (1963).
[12]G. H. Golub and J. H. Welsch, Math. Comput. 23, 221 (1969); I. P. Mysovskih, Dokl. Acad. Nauk SSSR 178, 1252 (1968) [Sov. Phys.-Doklady 9, 277 (1968)].
[13]R. K. Nesbet, J. Comput. Phys. 8, 483 (1971).
[14]J. H. Wilkinson, *The Algebraic Eigenvalue Problem* (Oxford U. P., New York, 1965), p. 229.
[15]R. A. Sack and A. F. Donovan, Numer. Math. 18, 465 (1972).
[16]H. Rutishauser, Proc. Symp. Appl. Math. 15, 219 (1963).
[17]E. Clementi and C. Roetti, At. Data Nucl. Data Tables 14 (1974); R. C. Raffenetti, J. Chem. Phys. 59, 5936 (1973).
[18]P. J. Leonard and J. A. Baker, in *Theoretical Chemistry, Advances and Perspectives,* edited by H. Eyring and D. Henderson (Academic, New York, 1975), Vol. 1, p. 117.
[19]H. B. G. Casimir and D. Polder, Phys. Rev. 73, 360 (1948).
[20]M. R. Aub and S. Zienau, Proc. R. Soc. A 257, 464 (1960).
[21]A. Dalgarno and W. D. Davison, Adv. At. Mol. Phys. 2, 1 (1966).
[22]R. E. Johnson, S. T. Epstein, and W. J. Meath, J. Chem. Phys. 47, 1271 (1967).
[23]E. R. Cohen and B. N. Taylor, J. Phys. Chem. Ref. Data 2, 663 (1973).
[24]T. N. E. Greville, in *Mathematical Methods for Digital Computers,* edited by A. Ralston and H. S. Wilf (Wiley, New York, 1967), p. 156.
[25]J. A. R. Samson, J. Opt. Soc. Am. 54, 876 (1964); Adv. At. Mol. Phys. 2, 177 (1966).
[26]J. F. Lowry, D. H. Tomboulian, and D. L. Ederer, Phys. Rev. 137, A1054 (1965).
[27]R. P. Madden and K. Codling, Phys. Rev. Lett. 10, 516 (1963).
[28]A. Dalgarno and A. E. Kingston, Proc. Phys. Soc. Lond. 78, 607 (1961); A. E. Kingston, Phys. Rev. 135, A1018 (1964).
[29]W. C. Martin, J. Res. Natl. Bur. Stand. (U.S.) A 64, 19 (1960).
[30]C. M. Moser, R. K. Nesbet, and M. N. Gupta, Phys. Rev. A 13, 17 (1976).
[31]W. J. Stevens and F. P. Billingsley II, Phys. Rev. A 8, 2236 (1973).
[32]P. K. Mukherjee, R. K. Moitra, and A. Mukherji, Int. J. Quantum. Chem. 5, 637 (1971).
[33]M. LeDourneuf and Vo Ky Lan (unpublished).
[34]C. E. Moore, *Atomic Energy Levels,* Natl. Bur. Stand. Circ. No. 467 (U.S. GPO, Washington, D.C., 1949);

H. E. Clearman, J. Opt. Soc. Am. 42, 373 (1952).
[35]J. M. Esteva, Ph.D. thesis (Univ. of Paris XI, 1974) (unpublished); J. M. Esteva, G. Mehlman-Balloffet, and J. Romand, J. Quant. Spectrosc. Radiat. Transfer 12, 1291 (1972).
[36]I. Bergström, J. Bromander, R. Buchta, L. Lundin, and I. Martinson, Phys. Lett. 28A, 721 (1969).
[37]G. M. Lawrence and B. D. Savage, Phys. Rev. 141, 67 (1966).
[38]J. Bromander, Phys. Scr. 4, 61 (1971).
[39]M. W. Smith and W. L. Wiese, Astrophys. J. 23, Suppl. No. 196 (1971).
[40]J. A. Kernahan, E. H. Pinnington, A. E. Livingston, and D. J. G. Irwin, Phys. Scr. 12, 319 (1976).
[41]A. R. Edmonds, *Angular Momentum in Quantum Mechanics* (Princeton U.P., Princeton, 1957).
[42]R. K. Nesbet, J. Math. Phys. 2, 701 (1961).
[43]E. U. Condon and G. H. Shortley, *The Theory of Atomic Spectra* (Cambridge U.P., New York, 1935).